NUCL SCI TECH (2019) 30:179
https://doi.org/10.1007/s41365-019-0703-2

Impact of atmospheric ionization by delayed radiation from high-altitude nuclear explosions on radio communication

Heng Xu[1] · Jian-Ming Ouyang[1] · Shang-Wu Wang[1] · Yun Liu[2] · Xu Sun[3]

Received: 10 December 2018 / Revised: 28 July 2019 / Accepted: 10 August 2019 / Published online: 19 November 2019

Abstract In this study, we investigated the motion, shape, and delayed radiation intensity of a radioactive cloud by establishing a volume-source model of delayed radiation after high-altitude nuclear explosions. Then, the spatial distribution of electron number density at different moments on the north side of the explosion point generated by delayed γ-rays and delayed β-rays from the radioactive cloud under the influence of the geomagnetic field was calculated by solving chemical reaction kinetics equations. The impact of radio communication in the different frequency bands on the process of atmospheric ionization was also studied. The numerical results of the high-altitude nuclear explosion (120 km high and with a 1 megaton equivalent at 40° N latitude) indicated that the peak of electron number density ionized delayed γ-rays is located at a height of approximately 100 km and that of electron number density ionized delayed β-rays is about 90 km high. After 1 min of explosion, the radio communication in the medium frequency (MF) and high-frequency (HF) bands was completely interrupted, and the energy attenuation of the radio wave in the very high-frequency (VHF) band was extremely high. Five minutes later, the VHF radio communication was basically restored, but the energy attenuation in the HF band was still high. After 30 min, the VHF radio communication returned to normal, but its influence on the HF and MF radio communication continued.

Keywords High-altitude nuclear explosions · Delayed radiation · Ionization effect · Radio communication

✉ Jian-Ming Ouyang
oyjm@nudt.edu.cn

1 College of Liberal Arts and Sciences, National University of Defense Technology, Changsha 410073, China

2 College of Physics and Micro Electronic, Hunan University, Changsha 410006, China

3 College of Electronics Science, National University of Defense Technology, Changsha 410073, China

1 Introduction

Nuclear explosions can be divided into underground, ground, airborne, and high-altitude nuclear explosions depending on the altitudes of their burst points. The difference in the height of the explosions leads to different explosion effects and damage factors [1]. High-altitude nuclear explosions are nuclear explosions that occur at a burst point higher than 30 km, which mainly radiate energy through X-rays, γ-rays, β-rays, and neutrons [2]. Because of the lower density of the atmosphere at high altitudes, the radiation generated from nuclear explosions can ionize the atmosphere in the range of thousands of kilometers, producing plasma to change the electromagnetic characteristics of the ionosphere, which could influence electromagnetic wave propagation. During 1958 to 1962, more than 10 high-altitude nuclear tests were conducted by the USA and U.S.S.R., which seriously affected the ionization layer and radio communication [3–6].

The ionization effects fall into two general categories: prompt ionization effects and delayed ionization effects. The prompt ionization sources are instantaneous point sources, including X-rays, prompt γ-rays, and neutrons, whereas delayed ionization sources are mainly continuous volume sources, such as delayed γ-rays and β-rays [7]. Although the effects of prompt ionization are strong, its duration is short (less than 10 μs), thus leading to no lasting impact on atmospheric ionization. However, the debris cloud formed after the high-altitude nuclear explosion could spread to thousands of kilometers and last for a considerable time, thus continuously affecting electromagnetic wave propagation and radio communication [8]. The process of the atmosphere ionized by delayed radiation can be divided into the following stages. The debris cloud formed after nuclear explosion spreads and rises, while the fissile fragments in the debris cloud continue to release delayed γ-rays and delayed β-rays. Then, the delayed γ-rays interact with atoms or molecules in the atmosphere, undergoing the photoelectric effect, Compton scattering, and electron pair effect, and generating high-energy electrons. This process is called the primary ionization process. High-energy electrons and delayed β-rays undergo the collision ionization effect with atoms or molecules under the influence of the geomagnetic field and produce low-energy electrons. This is called the secondary ionization process. These low-energy electrons get attached to other atoms or molecules to form negative ions, and then, the low-energy electrons or negative ions complex with positive ions. This attachment and compounding process is called the chemical reaction kinetics process. The propagation of electromagnetic waves in the atmospheric plasma generated from these processes could drive the movement of electrons toward energy loss and thus affect radio communication [9].

The structure, composition, and temperature of atmosphere are different at different altitudes, so the interaction processes between radiation and the atmosphere and the generation and consumption of electrons also vary. Obviously, the processes are very complicated, which poses a considerable challenge to modeling. In this study, a delayed radiation volume-source model was established to simulate the movement and evolution of the debris cloud first. Then, a model based on chemical kinetics equations [10] was set up to reveal details of the primary ionization processes, secondary ionization processes, and chemical reaction kinetics processes in the atmosphere. Lastly, the energy attenuation of different frequency bands of radio communication in the atmospheric plasma was calculated using Wentzel–Kramers–Brillouin (WKB) approximation [11].

2 Analytic model

The debris cloud formed after high-altitude nuclear explosions contains numerous fission fragments, which could spread to thousands of kilometers and continuously radiate delayed γ-rays and β-rays. Although the dose rate of delayed radiation is not as high as that of instantaneous radiation, the radiation can generate additional ionization of the ionosphere, thus affecting radio communication.

2.1 Delayed radiation volume-source model

After high-altitude nuclear explosions, the debris cloud spreads out and rises driven by a considerable share of energy. The cloud expands rapidly at the beginning and then engulfs the atmosphere. When the mass of the cloud is large enough, the driving process ends and the cloud is translated into diffusion with constant speed. Then, the cloud starts to gradually dilute. As mentioned above, there are some differences in the properties of the atmosphere at different altitudes, so the speed of diffusion is not the same in all directions. In general, the density of the atmosphere decays exponentially as altitude increases, so the cloud diffuses rapidly upward but slowly downward in the vertical direction. In the horizontal direction, the density of the atmosphere basically remains constant, so the debris cloud spreads out symmetrically. Therefore, the debris cloud is approximately inverted pear-shaped [12]. As the cloud spreads outward, its mass and geometric center also rise. The X-rays released at the beginning of the nuclear explosion heat the air to produce energy deposition below the explosion point. The buoyancy caused by the increase in the atmospheric temperature is greater than the gravity of the debris cloud itself, which leads to the rise of the debris cloud. The equations of motion for the diffusion and rise of the debris cloud are as follows

$$\rho(r)\frac{\mathrm{d}v_i}{\mathrm{d}t} = -\nabla p - v_i 4\pi R^2 \frac{\mathrm{d}R}{\mathrm{d}t}\rho_\mathrm{h}\xi\frac{\rho(r)}{M}, \tag{1}$$

$$M\frac{\mathrm{d}^2h}{\mathrm{d}t^2} = -\int p\cos\theta\mathrm{d}\sigma - Mg, \tag{2}$$

where R is the radius, h is the central height of the debris cloud, ρ_h is the atmospheric density of the explosion point, M is the total mass of the debris cloud, $\rho(r)$ is the density distribution in the debris cloud, r is the radius vector of one point in the debris cloud, p_h is the atmospheric pressure, v is the diffusion velocity, ξ is the probability of atmospheric molecules being involved, $\mathrm{d}\sigma$ is the surface element of the debris cloud, and θ is the angle between the normal of the panel and the vertical direction. The first term on the right side of Eq. (1) represents the pressure difference between the inside and outside of the debris cloud, and the second term represents the change in momentum caused by mass addition. The first item on the right side of Eq. (2) is the pressure difference between the upper and lower surfaces of the debris cloud, and the second term is the gravity of the debris cloud. As shown in Fig. 1, this model is used to calculate the horizontal diffusion radius of the debris cloud under the experimental parameters of “teak,” and the

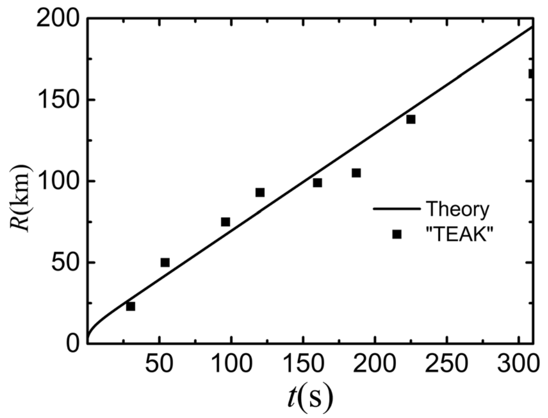

Fig. 1 Change of horizontal diffusion radius with time

theoretical calculation results agree well with the experimental values.

2.2 Delayed radiation ionization model

After 10 μs of the nuclear explosion, the delayed γ-rays begin to radiate. For the fission bomb, the radioactive intensity $A(t)$ (Ci) of γ-rays changing with time is given as

$$A(t) = b \times 10^{10} Q \frac{1}{t^n}, \tag{3}$$

where Q is the fission equivalent (kt), the value of b is between 4 and 8, and the value of n is related to t (min). When the value of t is less than 30 min, the value of n is 0.89. When the value of t is between 30 and 1440 min, the value of n is 1.11. When the value of t is greater than 30 min, the value of n is 1.26. For the same equivalent nuclear explosion, the radioactive intensity of delayed β-rays is 1.2–2.5 times larger than that of the delayed γ-rays, but the variation law of intensity with time is the same. The energy spectrum of the delayed γ-rays and β-rays can be obtained from a previous study [13].

The γ-rays emitted from fission fragments in the radioactive cloud undergo the photoelectric effect, Compton scattering, and electron pair effect with molecules or atoms in the atmosphere, generating high-energy electrons. Because the energy of γ-rays is not very high, the electron pair effect can be ignored. Simultaneously, the debris cloud keeps on releasing high-energy β-rays. These β-rays and high-energy electrons generated from reactions between γ-rays and particles in the atmosphere move spirally along the magnetic line of force in the geomagnetic field, undergoing the collision ionization effect with air particles in the zone of electron motion to consume themselves and generate secondary low-energy electrons. The geomagnetic field can be described by the magnetic dipole field as

$$\frac{B(h)}{B_0} = \frac{1}{(1 + h/R_{\mathrm{E}})^3}, \tag{4}$$

where R_{E} is the radius of the earth, and B_0 is the geomagnetic field intensity at 80 km, generally taken as 0.5 Gs. The gyration radius r_{g} of the high-energy electrons can be obtained from the following equation:

$$F_{\mathrm{L}} = \zeta m_{\mathrm{e}} \frac{v_{\mathrm{e}}^2}{r_{\mathrm{g}}}, \tag{5}$$

where F_{L} is the Lorentz force, ζ is the relativity factor, and m_{e} and v_{e} are the mass and velocity of the electron, respectively. Then, the ionization of the atmosphere near the magnetic field line can be obtained under the action of the Lorentz force.

As mentioned above, the process of photoelectric effect and Compton scattering between the γ-rays and air particles only produce high-energy electrons, and these high-energy electrons and β-rays undergo collision ionization with air particles to consume high-energy electrons. Therefore, the total generation rate of high-energy electrons could be written as

$$\frac{\mathrm{d}n_{\mathrm{eH}}}{\mathrm{d}t} = f_{\mathrm{com}}(n_{\mathrm{eH}}) + f_{\mathrm{pho}}(n_{\mathrm{eH}}) + f_{\mathrm{col}}(n_{\mathrm{eH}}), \tag{6}$$

where n_{eH} is the number density of high-energy electrons, f_{com} denotes the Compton scattering effect, f_{pho} denotes the photoelectric effect, and f_{col} denotes the consumption of high-energy electrons during secondary collision ionization processes. The Compton scattering process, the photoelectric effect process, and the secondary collision ionization process can all be considered two-body reactions [14]. The contribution to the generation of high-energy electrons of the three processes and parameters can be obtained from previous studies [11, 15–17].

The atmosphere ionized by delayed γ-rays and β-rays will produce a large number of low-energy electrons and ions. There are two processes for the loss of low-energy electrons. In one process, low-energy electrons complex with positive ions in the air directly, while in the other process, low-energy electrons attach to atoms or molecules to form negative ions, leading to a complex reaction with positive ions [18]. The atmosphere ionized by delayed γ-rays produces numerous low-energy electrons and ions. Considering 36 components and 229 reaction equations, the chemical reaction kinetics processes are very complex, including neutral particles (O, O_2, O_3, N, N_2, NO, NO_2, CO_2, H_2O, H, H_2, OH, and He), negative ions (e, O^-, O_2^-, O_3^-, O_4^-, CO_3^-, CO_4^-, $O_2^-{\cdot}H_2O$, $CO_3^-{\cdot}H_2O$, and $CO_4^-{\cdot}H_2O$), and positive ions (O^+, O_2^+, N_2^+, N_4^+, NO^+, O_4^+, H_2O^+, H_3O^+, H^+, He^+, $O_2^+{\cdot}H_2O$, $H_3O^+{\cdot}OH$, and $H_3O^+{\cdot}H_2O$). Therefore, the total change rate of low-energy electrons could be written as

$$\frac{dn_{eL}}{dt} = f_{chemL}(n_1, n_1, \ldots, n_{36}) - 2f_{col}(n_{eH}), \tag{7}$$

$$f_{chemL} = \sum_{j=1}^{36} \sum_{m=1}^{36} \varepsilon_{jm} k_{jm} n_j n_m, \tag{8}$$

where f_{chemL} is the term of chemical reaction kinetics, ε_{jm} is the generation consumption factor, k_{jm} is the reaction coefficient, and n_j and n_m are the number density of particles involved in chemical reactions. Because one high-energy electron can generate two low-energy electrons after collision ionization, the second term on the right of Eq. (7) is twice as much as consumption of high-energy electrons.

2.3 Attenuation of radio waves model

When electromagnetic waves are propagated in plasma, they will drive electrons to vibrate. The electrons collide with other particles to transmit energy, so that the electromagnetic waves generate energy attenuation. For non-magnetized cold collision plasma, the relative dielectric constant ε_r and propagation constant k are, respectively,

$$\varepsilon_r = n^2 = 1 - \frac{\omega_p^2}{\omega^2 + \upsilon^2} - j\frac{\upsilon}{\omega}\frac{\omega_p^2}{\omega^2 + \upsilon^2}, \tag{9}$$

$$k = k_0\sqrt{\varepsilon_r} = k_r + jk_i, \tag{10}$$

where n is the refractive index of the medium, ω is the incident angular frequency of the electromagnetic waves, υ is the collision frequency of the electrons with other particles, ω_p is the angular frequency of plasma collision, k_0 is the wavenumber in vacuum, k_r is the attenuation constant, and k_i is the phase constant. When the electromagnetic wave frequency is less than the plasma frequency, the electromagnetic wave is cut off. When it is greater than the plasma frequency, under the WKB approximation [19], the one-way energy attenuation Att (dB) of electromagnetic waves is given by

$$\mathrm{Att} = \left|10\lg\frac{P_h}{P_{h_0}}\right| = 8.69\left|\mathrm{Im}\left(\int_{h_0}^{h} k\mathrm{d}h\right)\right|, \tag{11}$$

where P_h and P_{h_0} are the energy of electromagnetic waves at a height of h km and h_0 km, respectively.

3 Results and discussion

After high-altitude nuclear explosions, low-energy electrons in the atmosphere are divided into the production process, continuous process, and consumption process. Because of the persistence of delayed radiation ionization, electrons are continuously produced. For the high-altitude nuclear explosions at an explosion height of more than 80 km, the laws of delayed radiation ionization are similar in many aspects, such as the change of energy deposition with height and the effect on radio communication. Therefore, a 120-km-high nuclear explosion with a 1-Mt explosion equivalent was selected as the research object to perform numerical simulations. We assumed that the explosion point is located at around 40° N, where the magnetic inclination of the geomagnetic field is 60°.

3.1 Distribution of electron density generated by delayed radiation ionization

As shown in Fig. 2, the distributions of electron number density at different moments after nuclear explosion are given. The solid lines represent the ionization caused by the delayed γ-rays, the dotted lines represent the ionization caused by the delayed β-rays, and the dots of different shapes represent the electron densities at different horizontal distances (100, 200, 500, and 1000 km) from the burst point following Earth's surface curvature.

After 1 min of nuclear explosion, the peak value of electron density generated by delayed ionization of γ-rays is located at a height of 100 km and the peak electron number density reaches 1×10^7 cm^{-3} at a radius of 100 km, which is higher by about three orders of magnitude than the background electron number density. As the horizontal distance increases, the electron number density gradually decreases. The peak electron number density at a horizontal distance of 1000 km is 1×10^6 cm^{-3}. However, the delayed β-rays only act on the atmospheric ionization within 200 km on the north side of the explosion point after 1 min of the nuclear explosion. The electron density of ionized delayed β-rays 100 km away from the north side of the explosion point is about 2×10^6 cm^{-3}, which is higher by one order of magnitude than the background electron density but lower by one order of magnitude than the electron density generated by delayed γ-rays.

After 5 min, the ionization range of the delayed β-rays extends to a horizontal distance of more than 1000 km, and the height of peak electron number density appears between 80 and 90 km. The main ionization that affected the height of delayed β-rays is located from 70 to 120 km. After 10 min, the peak electron number density generated by delayed γ-rays located at a horizontal distance of 100 km and at 100 km height is about 2×10^5 cm^{-3}, which is an order higher than the background atmospheric electron density. After 30 min of explosion, the ionization effect of delayed γ-ray starts to gradually weaken. At this time, the ionization effect of delayed β-rays becomes dominant, and the height of peak electron density is about 90 km. The electron number density is nearly well

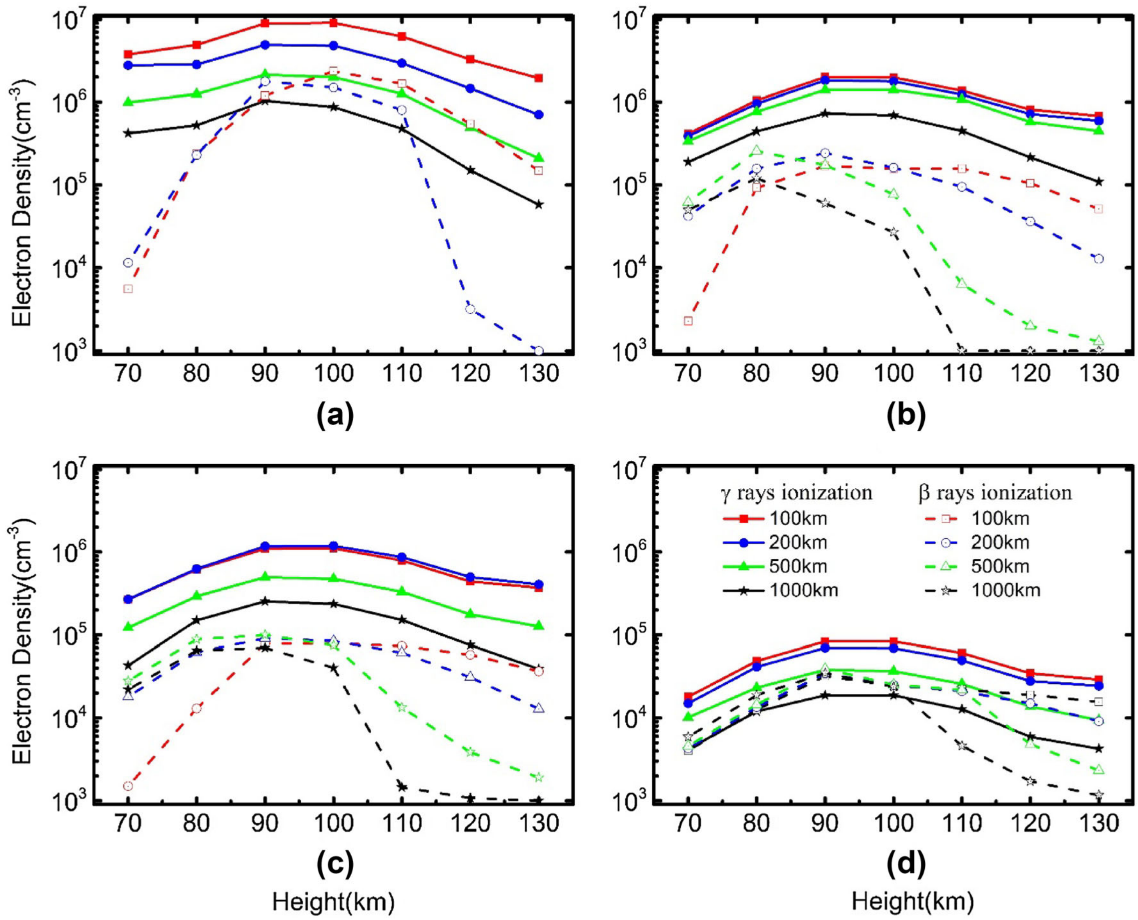

Fig. 2 (Color online) Number density of electrons generated by delayed γ-rays (solid line) and β-rays (dotted line) from a nuclear explosion at a 120 km explosion height and 1 Mt explosion equivalent at a 1 min, b 5 min, c 10 min, and d 30 min

distributed with the horizontal distance below a height of 100 km.

Figure 3 shows the spatial distribution of the electron number density generated by the total atmospheric ionization of delayed radiation on the north side of the explosion point at different moments after high-altitude nuclear explosions. The abscissa is the horizontal radius, and the ordinate is the vertical height. Because the density of the atmosphere near the explosion point is low, the spatial distribution center of the electron density caused by delayed radiation is located at a height of 90 km. As time progresses, the electron number density decreases. After 100 min, the electronic number density is 5×10^4 cm^{-3} and no more than 1×10^5 cm^{-3}.

3.2 Attenuation of radio waves by delayed radiation

When the electromagnetic wave frequency is greater than the plasma frequency, the electromagnetic wave can propagate in the plasma, and energy attenuation is noted in the process of propagation. When the electron number density is high enough, the incident electromagnetic wave frequency is lower than the plasma frequency. At this moment, the electromagnetic wave is in the off state and cannot propagate in plasma to produce reflection. The energy attenuation of radio wave decreases as the frequency increases. When the frequency of radio wave is low, radio communication is completely interrupted.

Figure 4 shows the effect of additional ionization generated by the delayed radiation on the high-frequency (HF) and very high-frequency (VHF) radio propagation after 1 min of the 120-km-high nuclear explosion with a 1 Mt explosion equivalent. In the range of 1000 km, the communication in the medium frequency (MF) band is completely interrupted, and the radio between 10 and 30 MHz is affected. The one-way energy attenuation of the radio wave with 25 MHz reaches 100 decibels at a horizontal distance of 100 km. The range of the effect of delayed radiation on the VHF radio communication is mainly within 200 km, and the attenuation of 120 MHz radio is about 10 decibels at a horizontal distance of 200 km.

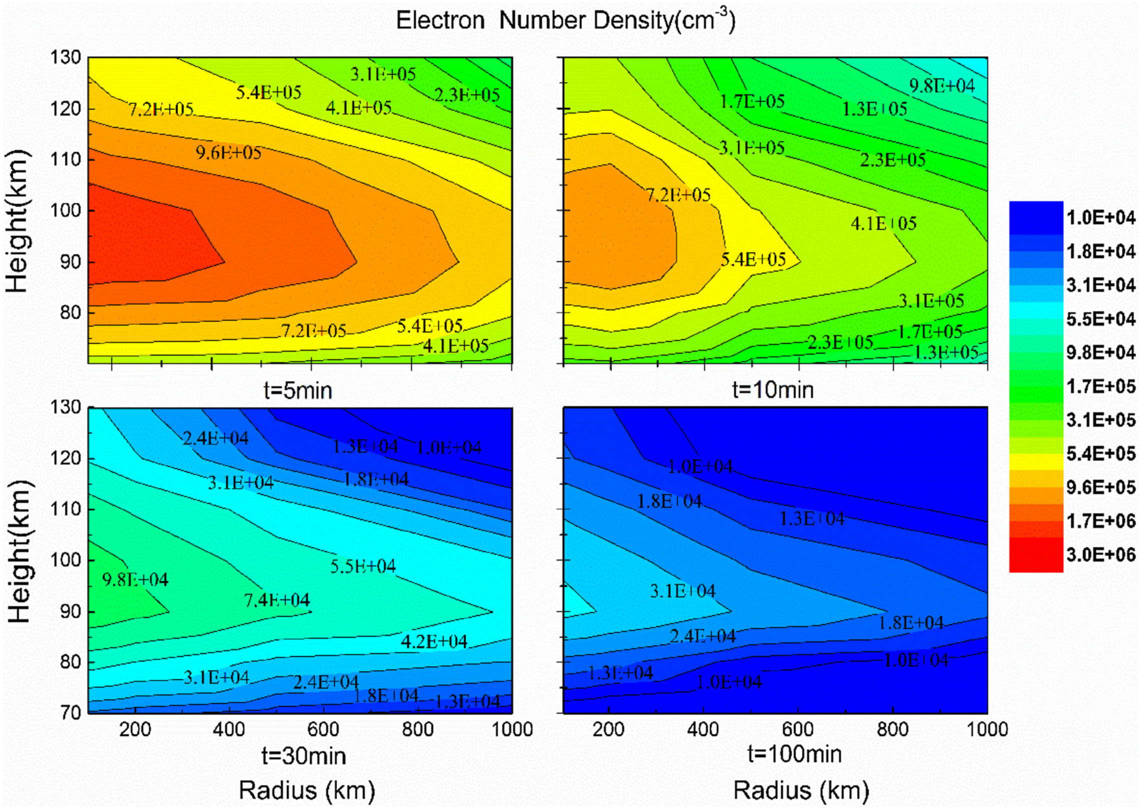

Fig. 3 (Color online) Distribution of electron number density on the north side of the 120-km high and 1-Mt equivalent nuclear explosion point

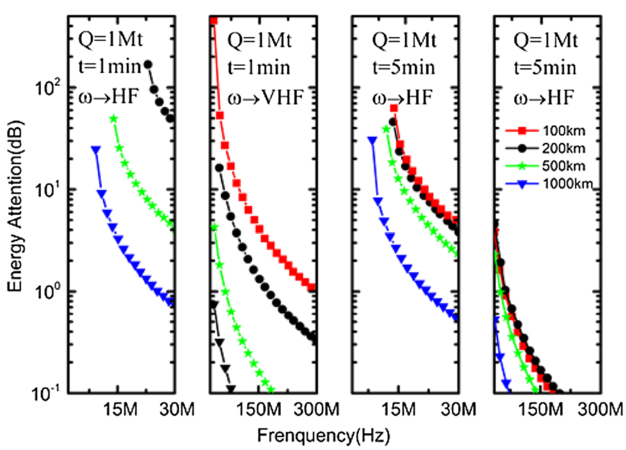

Fig. 4 (Color online) Energy attenuation of radio caused by delayed radiation from nuclear explosion

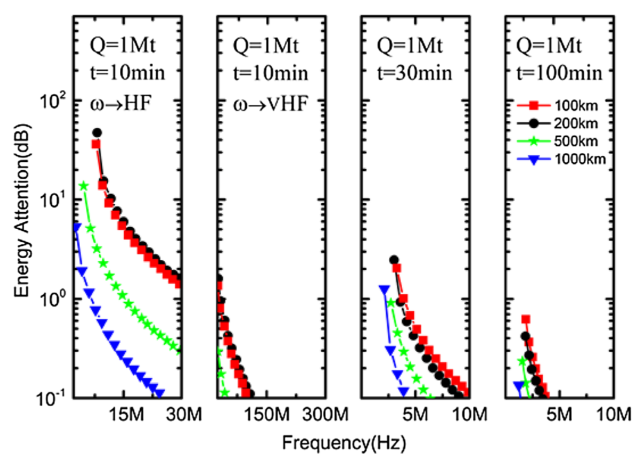

Fig. 5 (Color online) Energy attenuation of radio caused by delayed radiation from nuclear explosion

Figure 5 shows the energy attenuation of radio in some bands at some special moments. The radio communication energy attenuation in the VHF band reduces after 5 min, and a part of frequency communication is basically restored. The radio communication in the MF and HF band is still seriously affected, and the energy attenuation in the range of 500 km is higher than 10 decibels. Ten minutes later, the attenuation in the VHF band appears to be largely unaffected. The radio communication in the HF band is restored after 100 min.

4 Conclusion

In summary, to study the effect of additional ionization generated by delayed radiation in the atmospheric ionosphere on radio communication after high-altitude nuclear explosions, we built models in three stages. First, a delayed radiation volume-source model was established to simulate the diffusion and rise process of the debris cloud. Second, the electron number density generated by Compton scattering and the photoelectric effect between γ-photons and molecules or atoms in the atmosphere was calculated based on chemical kinetics equations. Furthermore, considering the geomagnetic field, the electron number density generated by the energy deposition of β-rays in the atmosphere on the north side of the explosion zone was also calculated. Third, the attenuation of the MF, HF, and VHF radio waves was estimated using WKB approximation, which provides references for the affected time and range of radio communication after high-altitude nuclear explosions.

The numerical results of the high-altitude nuclear explosions (120 km high and 1 Mt equivalent) 40° N show that the peak height of electron density generated by delayed γ-ray ionization is between 90 km and 100 km, and the peak value of the electron number density generated by β-ray ionization is located at around 90 km. Delayed radiation ionization lasts for a long time. The delayed γ-ray ionization dominated 10 min after the explosion. After 30 min, the ionization effect of the delayed β-rays exceeded that of the delayed γ-rays. One min after the explosion, the MF and HF radio communication were completely interrupted, and the VHF band radio wave attenuation was extremely high. After 10 min, the radio communication in VHF band was basically restored, whereas the energy attenuation of waves in the HF band was high. After 30 min, the radio communication in the VHF band returned to its normal state, but the attenuation of communication in the HF band was high.

References

1. D. Qiao, *The Introduction to Nuclear Explosion Physics* (National Defense Industry Press, Beijing, 2003), pp. 393–395
2. S. Glasstone, P.J. Dolan, *The Effects of Nuclear Weapons* (United States Department of Defense and the Energy Research and Development Administration, Washington, 1977), pp. 387–439.
3. H.P. Williams, The effect of high-altitude nuclear explosions on radio communication. IRE Trans. Mil. Electron. **6**(4), 326–338 (1962). https://doi.org/10.1109/IRET-MIL.1962.5008460
4. A.M. Petersen, Optical, electromagnetic and satellite observations of high-altitude nuclear detonations, part II. J. Geophys. Res. **64**, 933–950 (1959). https://doi.org/10.1029/JZ064i008p00933
5. H. Hoerlin, *United States High-Altitude Test Experiences*. (Los Alamos Scientific Laboratory, 1976), pp. 1–5.
6. C.H. Cummack, G.A.M. King, Disturbance in the ionospheric F-region following the Johnston Island nuclear explosion. N. Z. J. Geol. Geophys. **2**(3), 634–641 (1959). https://doi.org/10.1080/00288306.1959.10423166
7. J. Ouyang, Y. Ma, F. Shao et al., Ionization effect of atmosphere by prompt rays from high-altitude nuclear explosions. IEEE Trans. Nucl. Sci. **61**, 1143–1150 (2014). https://doi.org/10.1109/TNS.2014.2320595
8. Z. Sheng, *Advances in High Field Laser Physics* (Shanghai Jiao Tong University Press, Shanghai, 2014), pp. 2–15
9. S. Matsushita, On artificial geomagnetic and ionospheric storms associated with high-altitude explosions. J. Geophys. Res. **64**, 1149–1161 (1959). https://doi.org/10.1029/JZ064i009p01149
10. J. Ouyang, Y. Ma, F. Shao, D. Zou et al., The effect of energetic electron impact ionization on radiation ionization process of high-altitude nuclear explosion. Acta Phys. Sin. **61**, 212802 (2012). https://doi.org/10.7498/aps.61.212802
11. Z. Zhuang, N. Yuan, S. Liu et al., *Plasma Stealth Technology* (Science Press, Beijing, 2004), pp. 76–78
12. J. Wang, S. Niu, D. Zhang et al., *The Parameter Manual Book of High-Altitude Nuclear Explosion Effects* (Atomic Energy Press, Beijing, 2010), pp. 178–190
13. D. Qiao, *The Introduction to Nuclear Explosion Physics* (National Defense Industry Press, Beijing, 2003), pp. 399–401
14. J. Ouyang, W. Guo, L. Wang et al., Numerical simulation of chemical processes in one-dimensonal atmospheric plasmas. Acta Phys. Sin. **9**, 4975–4979 (2006). https://doi.org/10.7498/aps.55.4974
15. R.J. Vidmar, *Plasma cloaking: air chemistry, broadband absorption, and plasma generation*. (Remote Measurements Lab., CA, 1990), pp. 2–6.
16. J. Heicklen, *Atmospheric Chemistry* (Academic Press, Pittsburgh, 1976), pp. 40–42
17. G. Brasseur, S. Solomon, *Aeronomy of the Middle Atmosphere* (D. Reidel, Boston, 1984), pp. 353–355
18. D. Qiao, *The Introduction to Nuclear Explosion Physics* (National Defense Industry Press, Beijing, 2003), pp. 359–377
19. J. Zeng, J. Yuan, Radiative opacity of gold plasma studied by a detailed level-accounting method. Phys. Rev. E **74**, 025401 (2006). https://doi.org/10.1103/PHYSREVE.74.025401